

System-level Trade Study of Hybrid Parallel Propulsion Architectures on Future Regional and Thin Haul Turboprop Aircraft

Yu Cai*, Chrysoula L. Pastra[†], Jiacheng Xie[‡], Jasrayman K. Thind[§], Matheus M. Monjon[¶], Jonathan C. Gladin^{||}, and Dimitri N. Mavris^{**}

*Aerospace Systems Design Laboratory, Daniel Guggenheim School of Aerospace Engineering
Georgia Institute of Technology, Atlanta, Georgia, 30332*

This paper evaluates the potential benefits of applying hybrid parallel propulsion architectures to future turboprop aircraft that are expected to enter into service in 2030. Two baseline aircraft models are established by infusing viable 2030 airframe and engine technologies on state-of-the-art 19-passenger and 50-passenger aircraft models. Two parametric parallel hybrid architectures are proposed and applied on both size classes: Architecture 1 has two propellers, each driven by an engine and an electric motor in parallel, and allows in-flight recharging; Architecture 2 has four propellers, each driven by either an engine or an electric motor, and allows parallel operation during the cruise. A design space exploration is conducted on the powertrain design variables and the electric component key performance parameters. A constrained optimization implies that Architecture 1 and 2 can achieve fuel savings of about 2.6% and 6.6%, respectively, given 2030 electric component technology assumptions. Electric taxi consistently results in fuel saving when battery technology is beyond the projected 2030 level. Preliminary sensitivity studies show that the performance of Architecture 2 is more sensitive to the battery technology compared to Architecture 1 due to its extensive use of battery energy during the cruise.

I. Introduction

ELECTRIFIED aircraft propulsion (EAP) is at the epicenter of the future of aviation. It allows not only for more affordable and quieter flights but also for flights with a decreased or zero impact on the environment [1]. The goal of reducing or even eliminating conventional fuel consumption can be achieved by shifting toward electrified aircraft propulsion [2]. However, current battery technologies do not allow for fully electric large aircraft due to the low battery specific energy [1]. Future estimations of battery specific energy, specific power, and efficiency technological assumptions of electrified powertrain components, such as battery, electric motor, power converters, and generators [3–5], show that large fully electric aircraft are unlikely to be feasible in the near future due to the significant weight penalty associated with the electric powertrain, resulting in poor aircraft performance. Although full electrification of large aircraft is unlikely in the near future, hybrid electric aircraft are promising as they allow for a decrease in fuel consumption compared to the State of the Art (SoA) conventional aircraft [6, 7].

Hybrid-electric aircraft refer to those powered by an electric powertrain in combination with conventional gas turbine engines. There are multiple architectures that can be employed on hybrid-electric aircraft, including series, parallel, series-parallel, and turboelectric [8, 9], with series and parallel being more commonly seen in preceding studies [10, 11]. Each architecture has its own advantages and disadvantages, and some architectures may have their unique components. One of the major differences between series and parallel architectures is that series architectures require one or more turbogenerators [12]. These additional components add weight to the overall powertrain of a series architecture, which further constrains the hybridization. Additionally, the overall Maximum Takeoff Weight (MTOW) is increased causing a higher fuel consumption than the parallel powertrain. On the other hand, the series architecture also

*Senior Graduate Researcher, ASDL, Georgia Tech, AIAA Student Member

[†]Graduate Researcher, ASDL, Georgia Tech, AIAA Student Member

[‡]Graduate Researcher, ASDL, Georgia Tech, AIAA Student Member

[§]Graduate Research Associate, ASDL, Georgia Tech, AIAA Student Member

[¶]Graduate Research Associate, ASDL, Georgia Tech, AIAA Student Member

^{||}Senior Research Engineer, ASDL, Georgia Tech, AIAA Senior Member

^{**}S.P. Langley Distinguished Regents Professor and Director, ASDL, Georgia Tech, AIAA Fellow

allows for maximum thermodynamic efficiency, since the internal combustion engine operates at a constant speed and is characterized by simple powertrain control [13]. In comparison, parallel architectures enable the capability of splitting power demand for more power-intensive segments within the mission, while maintaining optimal propulsion system performance [13]. Since hybrid parallel architectures are likely to be more beneficial for the purposes of a regional turboprop aircraft due to its range and size [14], this paper will investigate the impact of parallel architectures on the sizing and performance of turboprop aircraft.

The research objective is to create parametric and physics-based models for two hybrid-electric regional turboprop aircraft and perform trade studies on different electrification settings. The hybrid-electric aircraft models were created in three phases. First, Technology Reference Aircraft (TRA) models are created for a 19-passenger and a 50-passenger aircraft based on public data. Then, viable 2030 airframe and engine technologies are infused on the TRA models to establish Advanced Technology Aircraft (ATA) models, which are used as the baselines to assess the impact of powertrain hybridization. Finally, The hybridized aircraft models are created by infusing two parallel hybrid-electric powertrains into the ATA models. With the parametric hybrid vehicle models, a design space exploration is performed to both assess the vehicle performance and investigate the impact of powertrain design variables and electric component technologies.

The remainder of this paper is organized as follows: Sec. II provides a summary of the modeling and simulation environment used in this study; Sec. III introduces the conventional baseline aircraft models to be integrated with hybrid-electric powertrains; Sec. IV discusses the development of two parallel hybrid-electric architectures; Sec. V defines the design space and shows the design space exploration results; Sec. VI draws the conclusion.

II. Modeling and Simulation Environment

Both the baseline and hybridized vehicles were evaluated in a multi-disciplinary design and analysis environment which enables sizing and performance evaluation of both conventional and advanced aircraft concepts. Figure 1 presents a high-level design structure matrix of the modeling and simulation (M&S) environment, generated using the pyXDSM package [15]. The primary inputs include the following:

- A notional aircraft configuration, including the vehicle layout, propulsion system architecture, etc.
- Point performance requirements, such as field length and rate of climb, which eventually translate to a design point described by the vehicle's takeoff power-to-weight ratio, P_{TO}/W_{TO} , and wing loading, W_{TO}/S_{ref}
- Mission performance requirements, such as the design payload, design range, and the mission profile

These inputs are parametric such that they can be varied within a range or a set in design space exploration to study the impact of certain design variables on selected metrics of interest.

The M&S environment is implemented in MATLAB. A notable feature is that the vehicle resizing optimizer and all disciplinary analyses are built modular as classes with object-oriented programming. Superclasses define common interfaces to ensure compatibility between the modules, and subclasses have customized data structure and behaviors (e.g., propulsion system sizing rules) that are specific to the tools used and aircraft system architecture of interest. In this study, the geometry scaling, aerodynamic analysis, and weight estimation are performed by NASA Flight Optimization System (FLOPS) [16, 17]; the integration of FLOPS as a submodule is realized by Sizing and Off-Design Mission Analysis (SODA), an in-house tool developed by Cai et al. [18, 19]. The gas turbine engine performance data are generated off-line from NASA Numerical Propulsion System Simulations (NPSS) [20] and are imported as look-up tables in the propulsion module to improve run time efficiency. The electric powertrain is modeled in MATLAB, to be discussed later in Sec. IV. The mission analysis is implemented with an energy-based approach in MATLAB, with the capability of performing payload-range analysis in conjunction with SODA. Owing to the flexibility in subclass implementation, the M&S environment is able to size and evaluate the performance of a variety of propulsion architecture concepts, including electrified propulsion.

In order to model the hybrid propulsion architecture, the propulsion module used in this study employs unique characteristics from Electrified Propulsion Architecture Sizing and Synthesis (E-PASS) [21, 22], which defines any propulsion system architecture by categorizing each propulsion subsystem into three general groups:

- **Thrust sources** represent subsystems whose primary function is to generate thrust given input power (e.g., propeller, fan, etc.)
- **Power sources** represent subsystems which generate primary (propulsive) power (e.g., internal combustion engine, electric motor, electric generator, etc.)
- **Energy sources** represent subsystems which store energy to be used by the primary power sources (e.g., fossil fuel, battery, hydrogen, etc.)

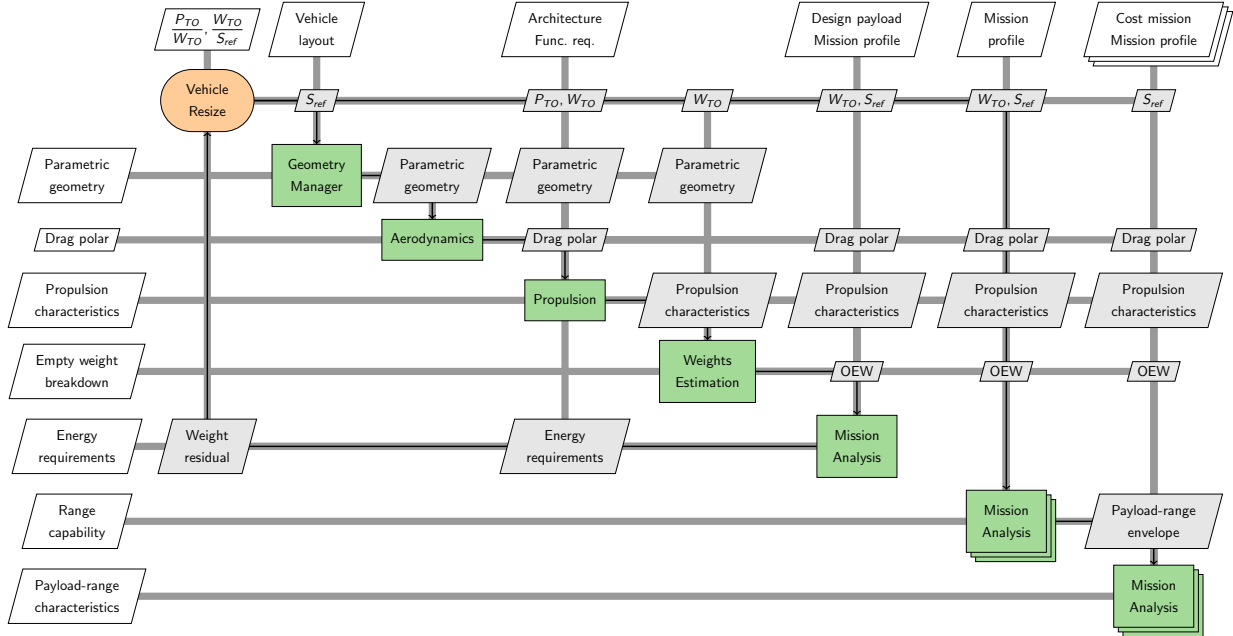


Fig. 1 Design structure matrix of the integrated modeling and simulation environment

The logical connectivity between these components and the power management at each mission segment can be described using a set of matrices [21, 22]. These matrices allow the computation of thrust requirement, power requirement, and energy consumption in power management functions, which are queried in the mission analysis module. Such an approach of propulsion architecture modeling is generic in that it can be used to model both conventional and hybridized propulsion systems.

III. Baseline Aircraft Models with Conventional Propulsion Architecture

A. Technology Reference Aircraft (TRA)

Two turboprop aircraft models were established as the Technology Reference Aircraft (TRA) based on public-domain data of SoA aircraft. The 19-pax thin haul model was calibrated based on the Beechcraft 1900D with a nominal range of 382 nmi carrying 19 passengers [23, 24]. The 50-pax regional aircraft model was calibrated based on the ATR 42-600 with a nominal range of 703 nmi with 48 passengers [25, 26]. The mission profiles of both aircraft are summarized in Tables 1 and 2. Details regarding the development of the TRA models can be found in Cai et al. [27].

B. Advanced Technology Aircraft (ATA)

To represent a target entry-into-service in the early 2030s, the advanced technology aircraft (ATA) models were created by infusing technologies expected to be mature by 2030 into the TRA models while retaining the conventional propulsion architecture. The selection of 2030 technologies considers the Technology Readiness Level, the effectiveness of the technology, and the compatibility of the technology with propeller-driven regional aircraft. As shown in Table 3, the technologies selected for advanced 19-pax and 50-pax models cover the disciplines of aerodynamics, structure, propulsion, and subsystems [28–37]. Details regarding these technologies can be found in Cai et al. [27]. The direct impacts of these technologies were parametrically modeled using scaling factors which act on certain aerodynamic, weight, and propulsive characteristics.

The technologies summarized in Table 3 were applied progressively to 19-pax and 50-pax aircraft. With a constant power-to-weight ratio, wing loading, and tail volume coefficients as the TRA, both aircraft were resized based on the same design mission. The associated technologies infused on the 19-pax and 50-pax TRA resulted in the cumulative

Table 1 19-pax mission profile (adapted from [27])

Segments	Description
Taxi-out*	Taxi for 6 min
Takeoff*	Take off and initial climb from sea level to 1500 ft for 1 min
Climb	Climb to 10 000 ft at 160 KEAS, then to 25 000 ft while linearly decelerating to 130 KEAS
Cruise	Level cruise at 167 KEAS
Descent	Descend to sea level at 200 KEAS
Approach	Descend to 1500 ft while decelerating to 160 KEAS
Missed approach*	Missed approach and climb to 5000 ft at 160 KEAS
Hold*	Level cruise at 160 KEAS for 5 min
Reserve climb	Climb to 15 000 ft using the same speed schedule as in the primary climb segment
Diversion	Level cruise at 160 KEAS
Reserve*	Level cruise at 160 KEAS for 45 min
Reserve descent	Descend to 5000 ft at 200 KEAS
Reserve approach*	Descend to 1500 ft while decelerating to 160 KEAS
Landing*	Final approach and landing for 3 min
Taxi-in*	Taxi for 4 min

* No distance credit

All descent segments are flown at a maximum flight path angle of 3 deg but may be shallower subject to idle thrust

Table 2 50-pax mission profile (adapted from [27])

Segments	Description
Taxi-out*	Taxi for 6 min
Takeoff*	Take off and initial climb from sea level to 1500 ft for 1 min
Climb	Climb to 25 000 ft at 160 KEAS
Cruise	Level cruise at 200 KEAS
Descent	Descend to 3000 ft at 200 KEAS
Approach*	Descend to 1500 ft while decelerating to 160 KEAS
Reserve climb	Missed approach and climb to 15 000 ft at 160 KEAS
Diversion	Level cruise at 200 KEAS
Reserve*	Level cruise at 200 KEAS for 45 min
Reserve descent	Descend to 3000 ft at 200 KEAS
Reserve approach*	Descend to 1500 ft while decelerating to 160 KEAS
Landing*	Final approach and landing for 3 min
Taxi-in*	Taxi for 4 min

* No distance credit

All descent segments are flown at a maximum flight path angle of 3 deg but may be shallower subject to idle thrust

Table 3 Selected 2030 technologies (adapted from [27])

Technologies	19-pax	50-pax
Riblets	✓	✓
Natural laminar flow	✓	✓
Variable-camber continuous trailing-edge flaps		✓
Flexible skins		✓
Excrescence reduction	✓	
Landing gear integration	✓	
Composite technologies	✓	✓
Advanced sandwich composites	✓	✓
Out-of-autoclave composite fabrication	✓	✓
Lightweight cabin furnishing		✓
Advanced engine cycle	✓	✓
Advanced engine components	✓	✓

impact on gross weight, operating empty weight, and block fuel outlined in Table 4. For both ATA models, a significant block fuel reduction is achieved mostly due to the advanced engines ($\approx -14.5\%$), natural laminar flow, and composite technologies. The individual impacts of each technology on the key performance and geometry metrics of the ATA in comparison to the TRA can be found in Cai et al. [27].

Table 4 Overall impact of technology infusion (adapted from [27])

Impact	19-pax	50-pax
Takeoff gross weight	-10.3%	-13.0%
Operating empty weight	-10.3%	-14.2%
Design mission block fuel	-30.2%	-32.9%

C. Optimized Design Point for ATA Models

Following the technology infusion, the design mission was also updated for both aircraft based on recent literature: for the 19-pax aircraft, the weight per passenger was increased from 210 lb (95.3 kg) to 215 lb (97.5 kg) based on the latest FAA advisory circular; for the 50-pax aircraft, the design range was reduced from 703 nmi to 500 nmi based on historical operational data [38]. To assess the impact of technologies and mission change, a parametric sweep was performed by varying the sea-level power-to-weight ratio and takeoff wing loading and resizing the vehicle at each point. As presented in previous work [27], a constraint diagram was generated for both vehicles, and the new design point was selected by minimizing the block fuel subject to the same climb and landing constraints as the TRA model. The selected design point for the 19-pax and 50-pax aircraft and their associated key performance and geometry specifications are summarized in Table 5. These optimized ATA models are used as the reference for comparisons with the hybrid-electric propulsion architectures.

IV. Development of Parallel Hybrid-Electric Architectures

A. Architecture 1

Architecture 1 has been proposed in a previous study [39]. As shown in Fig. 2(a), the architecture utilizes a configuration consisting of two propellers, each connected to a gas turbine engine and an electric motor in parallel via a power split unit. The electric motors are connected to a universal battery pack of lithium-ion cells. Considering different mission segments, four operational modes are defined for this architecture:

Table 5 High-level comparison between Technology Reference Aircraft (TRA) models and Advanced Technology Aircraft (ATA) models [27]

Item	Unit	19-pax			50-pax		
		TRA	ATA	Change	TRA	ATA	Change
Design range	nmi	382	382	–	703	500	–28.9%
Design payload	kg	1810	1853	+2.4%	4560	4560	–
Power-to-weight ratio	kW/kg	0.2441	0.2332	–4.5%	0.1731	0.1600	–7.6%
Maximum takeoff weight	kg	7815	7056	–9.7%	18 600	15 654	–15.8%
Operating empty weight	kg	4932	4429	–10.2%	11 700	9846	–15.8%
Wing planform area	m ²	28.8	26.0	–9.7%	54.5	45.9	–15.8%
Wing span	m	17.6	16.7	–5.1%	24.6	22.5	–8.5%
Engine rated power, each	kW	954	823	–13.7%	1610	1252	–22.2%
Block fuel at ATA design range	kg	579	402	–30.6%	1147	744	–35.1%
Cruise average BSFC	kg/kW/h	0.3249	0.2867	–11.8%	0.2817	0.2488	–11.7%
	lbm/hp/h	0.5341	0.4713	–11.8%	0.4631	0.4090	–11.7%
Cruise average TSFC	g/N/s	0.012 65	0.011 09	–12.3%	0.013 02	0.011 58	–11.1%
	lbm/lbf/h	0.4466	0.3914	–12.3%	0.4597	0.4087	–11.1%

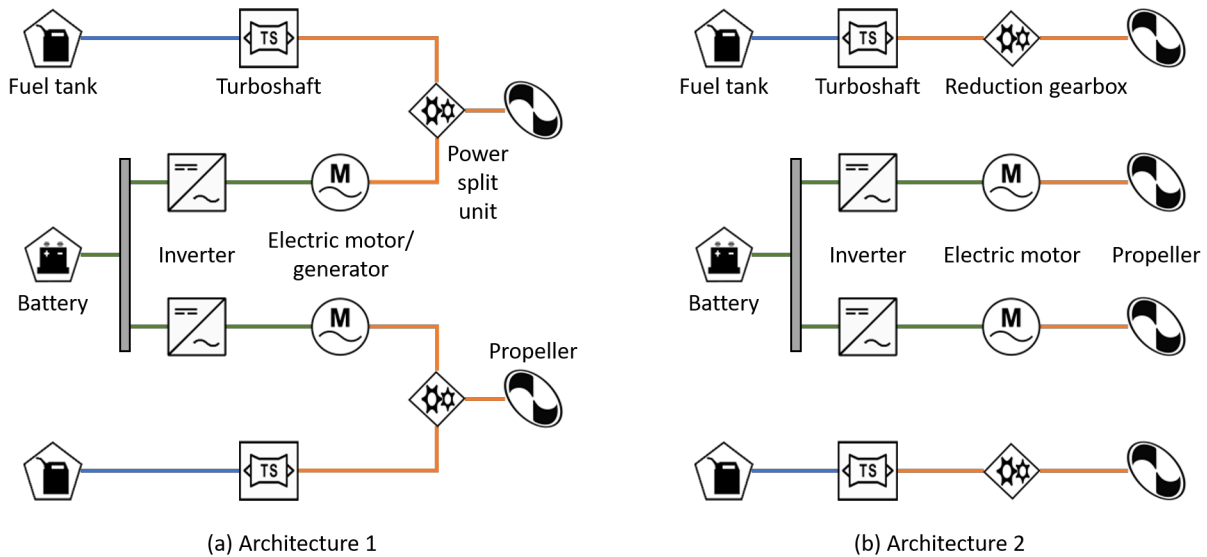


Fig. 2 Logical connectivity of proposed parallel architectures

- 1) **Hybrid-electric mode:** Each propeller is driven by both the gas turbine engine and the electric motor. The power management strategy (i.e., power split) is predetermined for the design mission profile and may not be of constant amount, timing, and duration for a specific flight segment. This mode is only used in the takeoff and climb segments of the primary mission. During the takeoff, all power sources are operating at their rating powers. During the climb, turboprop engines continue to operate at the rated power while electric motors are operating at a prescribed power code (i.e., percentage of rated power). Such boosting can occur over a prescribed altitude interval at either the beginning or the end of the climb segment.
- 2) **Fuel-only mode:** The propellers are driven exclusively by turboprop engines, while electric motors are turned off. This mode is primarily used in the cruise, descent, and landing of the primary mission, the unboosted part of the climb segment of the primary mission, and the entire reserve mission.
- 3) **Recharging mode:** When the battery is not fully charged and turboprop engines have available excess power, the electric motors may be reversely driven by the engines and behave as generators, converting mechanical power into electric power, thus charging the battery. Note that subject to the engine's excess power, the actual charging rate may be lower than the predefined desired charging rate. This mode is primarily used in the cruise and descent segments of the primary mission.
- 4) **Full-electric mode:** The propellers are driven exclusively by electric motors while turboprop engines are turned off. This mode is only used in taxi segments if an E-taxi strategy is desired.

The sizing of the turboprop engine and electric motor is subject to the following constraints:

- 1) **Sea-level power requirement:** Given a sea-level electric power fraction (λ_{SL}), the rated power of each engine ($P_{eng,SL}$) and electric motor (P_{em}) must satisfy the sea-level power requirement derived from the maximum takeoff weight (W_0) and power-to-weight ratio (P_{TO}/W_0):

$$P_{eng,SL} \geq \frac{1 - \lambda_{SL}}{2} \cdot \frac{P_{TO}}{W_0} \cdot W_0 \quad (1)$$

$$P_{em} \geq \frac{\lambda_{SL}}{2} \cdot \frac{P_{TO}}{W_0} \cdot W_0 \quad (2)$$

- 2) **Top-of-climb requirement:** At the cruise altitude and climb speed, with electric motors turned off, turboprop engines must be able to provide sufficient excess power for a climb rate of 300 ft/min. As a conservative approach, this constraint is evaluated at the maximum takeoff weight.
- 3) **Cruise requirement:** At the cruise altitude and cruise speed, with electric motors turned off, turboprop engines must be able to provide sufficient power to sustain a steady level flight. As a conservative approach, this constraint is evaluated at the maximum takeoff weight.
- 4) **E-taxi requirement:** If E-taxi is desired, electric motors must satisfy the critical thrust requirement, which accounts for the rolling friction force, a 1.5% uphill slope, and an acceleration from zero to 20 kts in 10 sec (for runway crossing).

It is noted that if constraint 2 or 3 is active, the relevant power sources may be oversized with respect to the sea-level power requirement. The corresponding penalty in weights and energy consumption, if any, will be reflected in the vehicle performance.

B. Architecture 2

Architecture 2 also includes two turboprop engines and two electric motors. In contrast to Architecture 1, this architecture is equipped with four propellers with each of them connected to either an engine or an electric motor, as depicted in Fig. 2(b). Due to the lack of mechanical connection between the engines and the electric motors, this architecture does not support in-flight recharging. Three operational modes are defined for this architecture:

- 1) **Hybrid-electric mode:** All four propellers and the corresponding power sources are operating to provide thrust based on the thrust requirement T_{req} and a prescribed target thrust split λ_T . The actual thrust distribution (T_1, T_2 ,

T_3 , and T_4) is obtained by solving the following optimization problem at every time step:

$$\min_{\tau} \left(\sum_{i=1}^4 T_i(\tau) - T_{\text{req}} \right)^2 \quad (3)$$

$$\text{s.t. } T_1(\tau) = \text{median} \{T_{1,\text{min}}, T_{1,\text{max}}, \tau \cdot (1 - \lambda_T)/2\} \quad (4)$$

$$T_2(\tau) = \text{median} \{T_{2,\text{min}}, T_{2,\text{max}}, \tau \cdot (1 - \lambda_T)/2\} \quad (5)$$

$$T_3(\tau) = \text{median} \{T_{3,\text{min}}, T_{3,\text{max}}, \tau \cdot \lambda_T/2\} \quad (6)$$

$$T_4(\tau) = \text{median} \{T_{4,\text{min}}, T_{4,\text{max}}, \tau \cdot \lambda_T/2\} \quad (7)$$

where T_1 and T_2 are the thrust per propeller driven by the engines, T_3 and T_4 are the thrust per propeller driven by the electric motors, and subscripts “min” and “max” indicate the minimum and maximum thrust available within the limits of the respective power sources. The hybrid-electric mode is used primarily in takeoff, climb, cruise, and landing segments. Effectively, in the takeoff and climb segments where the desired thrust is $+\infty$, all power sources operate at their prescribed power codes; in cruise and landing segments with finite thrust requirements, the optimizer will attempt to distribute the thrust based on λ_T while ensuring force balancing. Specifically, if λ_T is too low, the optimizer will command the engines to operate at full power while dynamically adjusting the power of electric motors to satisfy the thrust requirement; similarly, if λ_T is too high, the electric motors will operate at full power, while the engine power will be adjusted to satisfy the thrust requirement.

- 2) **Fuel-only mode:** The electric motors are turned off, and the respective propellers are assumed to be folded to minimize parasite drag. This mode is used in the descent segment of the primary mission, the entire reserve mission, and taxi segments if an E-taxi strategy is not desired.
- 3) **Full-electric mode:** The turboprop engines are turned off, and only the propellers connected to the electric motors are operating. This mode is only used in taxi segments if an E-taxi strategy is desired.

The sizing of the turboprop engine and electric motor is subject to the following constraints:

- 1) **Sea-level power requirement:** This requirement is identical to that of the first architecture.
- 2) **Top-of-climb requirement:** At the cruise altitude and climb speed, with the electric motors operating at a prescribed power code, the propulsion system must be able to provide sufficient excess power for a climb rate of 300 ft/min. As a conservative approach, this constraint is evaluated at the maximum takeoff weight.
- 3) **Cruise requirement:** At the cruise altitude and cruise speed, with all power sources operating, the propulsion system must be able to provide sufficient power to sustain a steady level flight. As a conservative approach, this constraint is evaluated at the maximum takeoff weight.
- 4) **E-taxi requirement:** This requirement is identical to that of the first architecture.

C. Electric Machine and Power Converters

As shown in Fig. 2, both electrified powertrains consist of a battery, inverters, electric motors, and cables. To be consistent with the technologies infused in the ATA models, electrical components were modeled considering the technological improvements projected in the 2030 to 2050 time frame. As summarized in Table 6, according to Pastra et al. [4], in 2050, the specific power of the electric motor could reach up to 11.3 kW/kg with a conservative projection or 50 kW/kg with an aggressive projection. Additionally, the efficiency of the electric motor could reach up to 97.0% with a conservative projection or 98.9% with an aggressive projection. The projection of the power converter specifications can be found in Hall et al. [5], as summarized in Table 7. The specific power of the converter could reach up to 12 kW/kg to 52.9 kW/kg depending on the conservative or aggressive projection model, and the efficiency of the converter could reach up to 98.7% to 99.7% depending on the conservative or aggressive projection model.

D. Battery Model and Battery Sizing

The battery used in the hybridized powertrain is modeled as a battery pack in which a number of battery cells are arranged in serial or parallel and connected by wires. As shown in Fig. 3 the pack-level specific energy is linearly correlated to the cell-level specific energy. For both the 19-pax and 50-pax models, the linear correlation between the battery pack-specific energy and cell-level specific energy has a 1% and 0.53% root mean squared error (RMSE), respectively. The weight of the battery includes the weight of the battery cells but also a packaging weight that includes the battery module housing, cooling system, battery management systems, and intra- and inter-module wires. The weights per length of wires are determined using Tables 310.15(B)(1) and 310.15(B) in the National Electrical Code [40]. All the battery components are automatically sized with the sizing of the battery capacity at the pack level.

Table 6 Electric machine specific power and efficiency projection [4]

Timeframe	Confidence Level	Specific Power (kW/kg)	Efficiency
SoA	-	6.0	0.960
2030	Conservative	9.2	0.963
	Nominal	13.2	0.968
	Aggressive	16.1	0.974
2040	Conservative	10.8	0.967
	Nominal	20.4	0.975
	Aggressive	33.0	0.983
2050	Conservative	11.3	0.970
	Nominal	24.3	0.980
	Aggressive	50.0	0.989

Table 7 Power converter specific power and efficiency projection [5]

Timeframe	Confidence Level	Specific Power (kW/kg)	Efficiency
SoA	-	7.5	0.980
2030	Conservative	9.6	0.980
	Nominal	13.8	0.985
	Aggressive	17.3	0.988
2040	Conservative	11.4	0.985
	Nominal	21.1	0.989
	Aggressive	35.1	0.994
2050	Conservative	12.0	0.987
	Nominal	25.2	0.992
	Aggressive	52.9	0.997

The battery capacity is sized by the mission analysis, as illustrated by Fig. 4. At the starting point, an initial estimation of battery capacity is given to run the mission analysis. In the mission analysis, the energy consumed from the battery is determined by integrating the power required by the electric motors at each time divided by the product of efficiencies of all electric components. In the discharging process, the energy flows from the battery to the propellers through the energy/battery cable, HV/DC, motor cable, inverter, and electric motors. For Architecture 1, the in-flight charging flow from the turboprop engines to the battery is the reverse of the discharging flow. The battery sizing is subjected to two constraints: the minimum state of charge and the maximum current. If the state of charge of the battery is lower than 20% at the end of the mission or the actual battery current exceeds the maximum limit, the battery will be up-sized and re-run the mission analysis. If the state of charge of the battery is higher than 20% at the end of the mission and the actual current is lower than the maximum limit, the battery will be downsized and re-run the mission analysis. This process will keep iterated until one of the following conditions is met:

$$\text{SoC} = 20 \quad \& \quad I \leq I_{max} \quad (8)$$

$$\text{SoC} \geq 20 \quad \& \quad I = I_{max} \quad (9)$$

Finally, the sized battery capacity will be rounded up to a whole number of modules.

E. Gas Turbine Engine Models

The turbine engine performance, size, and weight should be considered along with the other components of the vehicle for the optimized performance of future hybrid electric aircraft. A “scalable” engine model is used to predict the expected performance and weight of the new centerline engines over a continuous range of design power levels.

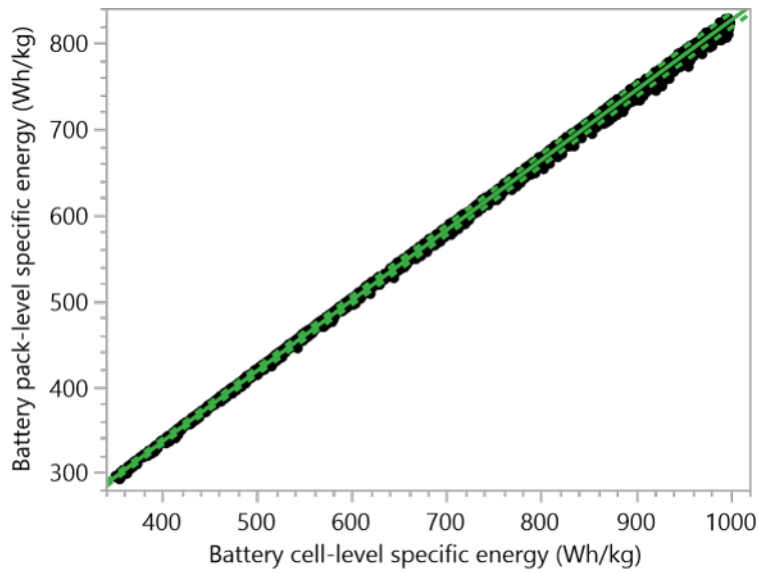


Fig. 3 Correlation between cell-level specific energy and pack-level specific energy for battery pack

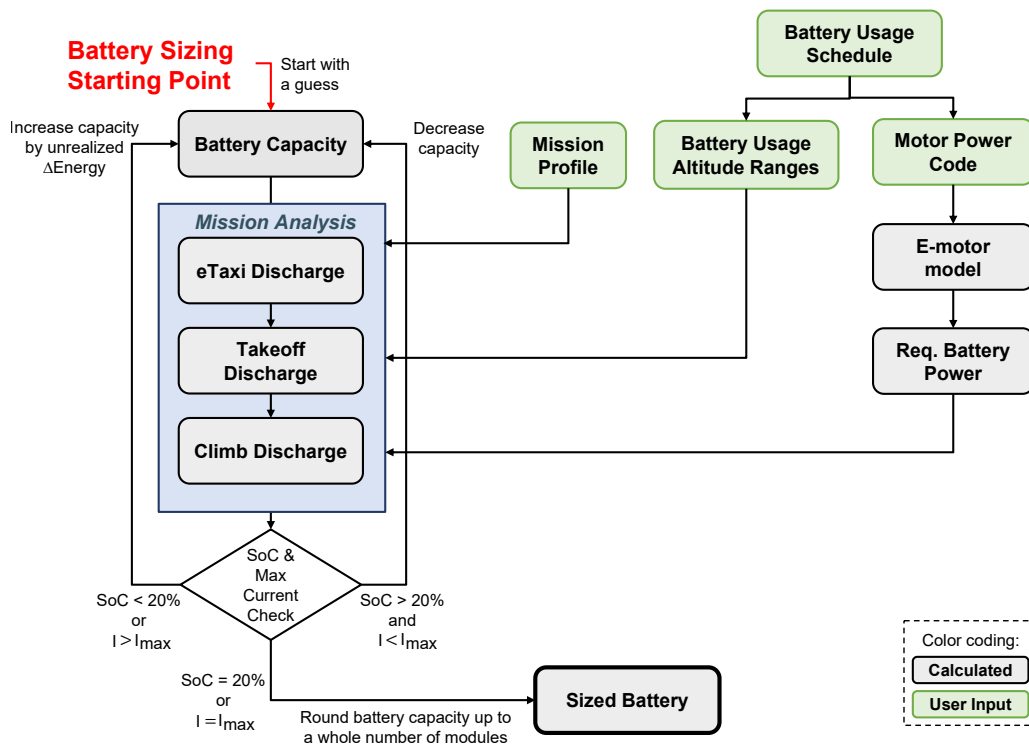


Fig. 4 Battery sizing logic [41, 42]

The NASA Numerical Propulsion System Simulation (NPSS) [20] was used to develop the scalable engine model. The current engine data available from open literature was represented by a “baseline” scalable model, which does not match the performance of any specific engine(s), rather it is an indication of current engines with similar design power levels. All engines represented by this “baseline” scalable model have the same architecture and characteristics i.e. a single spool gas generator with an axi-centrifugal compressor and a free power turbine.

To represent the expected performance and weight of future engines the scalable baseline model was adjusted according to future performance trends from several published sources [37, 43, 44]. The engine cycle is assumed to vary with engine design power, through the design overall pressure ratio (OPR) and turbine inlet temperature (T4). Evolutionary improvements in component aerodynamics and turbine cooling in combination with the incorporation of new technologies such as CMC materials and 3D manufacturing lead to significant performance improvements. An algorithm developed by Gauntner [45] is used to estimate the turbine cooling flows. Finally, the coupling of the top-of-climb power requirement and the sea level calibration point are achieved by multiple design point (MDP) methods [46]. The three design points are defined as follows:

- **Sea level takeoff:** calibration point; sets design power, OPR, and T4
- **Hot day:** engine power is flat-rated to a 95°F day; sets turbine cooling and T4 limit
- **Top-of-climb:** engine is sized to provide required power at top-of-climb (TOC)

A guess for the sea-level takeoff power initiates the iterations in the MDP design and is also used in combination with pre-defined correlation curved to select the design OPR and T4. Hot day conditions reused to define the maximum T4 and to size the turbine cooling flows. Maximum climb power is maintained until T4 is limited by altitude, after which power decreases. Convergence of the iteration on sea-level power occurs when the required top-of-climb power is achieved. The TOC condition is also used to set all of the component efficiencies. Once the engine design is completed, off-design performance data is generated and is fed back to the vehicle system model. This procedure is repeated for a variety of engine design power levels, as required during the vehicle level design iteration.

F. Propeller Sizing and Performance Evaluation

For all vehicle models including the ATA, each propeller is sized to maintain the same disk power loading as in the respective TRA model. The propeller speed (RPM) is varied following change in the diameter to maintain the same advance ratio. The propeller mass is estimated using the adjusted Torenbeek method based on Ref. [47]:

$$m_{prop} = k \left(D_p P_{max} \sqrt{B} \right)^{0.52} \quad (10)$$

where D_p is the propeller diameter in meters, P_{max} is the maximum shaft power in kilowatts, B is the number of blades, and m_{prop} is the propeller mass in kilograms. A multiplicative factor k is used to calibrate the propeller mass against the TRA data.

The propeller performance is evaluated based on the Hamilton Standard database [48]. In the M&S environment, the propeller model has the following nondimensional functional form:

$$C_T = f(J, C_P)|_B \quad (11)$$

where $J = V_\infty/nD_p$ is the advance ratio, $C_P = P_{in}/\rho n^3 D_p^5$ is the power coefficient, and $C_T = T/\rho n^2 D_p^4$ is the thrust coefficient. For both the 19-pax and the 50-pax models, the nondimensional propeller model is invariant during resizing. While the propellers operate at constant speed for most phases, the propeller speed is varied between 40% and 100% of takeoff setting to minimize power requirements during E-taxi [39].

V. Design Space Exploration

A. Design Space Definition

A design space exploration is conducted to understand the impact of hybrid powertrain design variables and electric component technologies on vehicle sizing and mission performance. Among the system-level design variables shared between both architectures, “sea-level electric power fraction” (λ_{SL}) describes the fraction of required sea-level takeoff power to be provided by the electric motors, as defined in Sec. IV.A. “E-taxi switch” is a binary variable specifying whether an electric taxi is desired for the design mission. The system design voltage determines the stack voltage of the battery pack, affecting the sizing of the battery.

Table 8 Ranges of the considered design variables for both hybrid parallel architectures

Design Variable	Unit	Architecture 1	Architecture 2
Sea-level electric power fraction	–	0.05 - 0.25	0.10 - 0.30
Cruise target thrust split	–	N/A	0.05 - 0.95
Climb boosting type	–	High/Low	N/A
Total boosting altitude	ft	0 - 25 000	N/A
Electric motor power code at climb	–	50 - 100	70 - 100
Recharging during cruise	–	On/Off	N/A
Recharging speed	C	0.5 - 2.0	N/A
E-taxi switch	–	On/Off	On/Off
System design voltage	V	540 - 1260	540 - 1260
Battery cell-level specific energy	Wh/kg	300 - 1000	300 - 1000
Electric motor specific power	kW/kg	3 - 30	3 - 30
Inverter specific power	kW/kg	5 - 50	5 - 50
Electric motor efficiency	–	0.95 - 1.00	0.95 - 1.00
Inverter efficiency	–	0.95 - 1.00	0.95 - 1.00

During the climb boost, the electric motors in both architectures operate at a prescribed power code (i.e., percentage of the rated power). For Architecture 1 only, since the engines alone are sized to satisfy the top-of-climb power requirement, the climb can be partially boosted to reduce battery size; this is parameterized by a total boosting altitude, which ranges from zero to cruise altitude, and a binary variable to indicate whether the climb boost takes places at low altitude (as a continuation of takeoff boost) or high altitude (towards the end of the climb).

To characterize the in-flight battery recharging of the first architecture, two design variables are defined: “recharging during cruise” and “recharging speed”. The former is a binary variable specifying whether the battery is to be recharged at the cruise segment aside from the descent segment. The latter specifies how fast the battery is being recharged in terms of C-rate. As described in Sec. IV.D, the actual charging speed will be limited by the engine excess power available.

Different from Architecture 1, the true-parallel nature of Architecture 2 does not allow in-flight recharging but instead allows the use of electric motors at the cruise segment, where the design variable “target electric power fraction” (i.e., the λ_T described in Sec. IV.B) specifies the desired thrust split between the engine-driven propellers and the motor-driven propellers.

The last set of input variables is the key performance parameters of electric components, including the specific energy of the battery cell and the specific power and efficiency of the electric motor and power inverter. These variables are included to assess the impact of electric component technologies on vehicle-level performance and variation of the best-performing design.

B. Design Space Exploration and Sensitivity Analysis

Since it takes approximately 2-3 min to evaluate a single design in the M&S environment on a typical personal computer, it is prohibitive to directly run the environment for design space exploration. Instead, a Design of Experiments (DoE) consisting of 6000 Latin hypercube sample points for each architecture and size class is created based on the ranges defined in Table 8. This allows each sample point to be evaluated in the M&S environment in parallel. The responses of interest include the following:

- **Climb performance:** This is characterized by the sea-level rate of climb in “all-engine-operating” condition and the time to climb to cruise altitude. With hybrid-electric architectures, “all-engine-operating” means that both the engines and the electric motors are operative. The climb performance is primarily used as a constraint to filter out infeasible designs.
- **Powertrain performance:** This includes the average cruise brake specific fuel consumption (BSFC, ratio of engine fuel flow to engine output shaft power), average cruise thrust specific fuel consumption (TSFC, ratio of *total fuel flow to total net thrust*), and taxi thrust excess ($\log(T_{av}/T_{req})$ at taxi segment). The definition of specific

fuel consumption is generalized based on similar concepts for conventional aircraft to allow direct comparison between the ATA and the hybridized aircraft. The taxi thrust excess serves as a constraint to filter out infeasible designs.

- **Weights and mission performance:** This includes the battery pack weight, the takeoff gross weight (TOGW), the operating empty weight (OEW, battery excluded), and the block fuel and block energy of the design mission, where the block energy is the sum of the energy of block fuel (based on a lower heating value of 11.9 kWh) and the effective battery energy consumed (i.e., zero if the battery is fully recharged at the end of the mission). These metrics are primarily used as design objectives.

After the results have been collected, surrogate models are established between response metrics and design variables to enable fast evaluation of any points within the design space. For each response, a two-layer artificial neural network (ANN) model is created and validated using a 5-fold cross-validation method; a minimal number of neurons are selected to achieve high R-squared values (above 0.99) and small root mean squared error (within 0.5%) for both the training set and the validation set. Using the surrogate models, interactive prediction profilers are generated to visualize and explore the trends between the design variables and responses of interest, where each cell is a plot showing the response of a single output to the variation of a single input while holding all other inputs at their current settings.

The following subsections present a snapshot of the prediction profiler for each size class and architecture, where the powertrain design variables except the system design voltage are selected to minimize the design mission block fuel, while the system design voltage is fixed at 1080 V and the electric component technological parameters take the settings in Table 9 to represent a nominal 2030 technology level.

Table 9 Assumptions of 2030 electrified powertrain technology levels

Parameter	Value	Unit	Ref.
Battery cell-level specific energy	489	Wh/kg	[3]
Electric motor specific power	13.2	kW/kg	[4]
Inverter specific power	13.8	kW/kg	[5]
Electric motor efficiency	0.968	–	[4]
Inverter efficiency	0.985	–	[5]

1. 19-pax Vehicle with Architecture 1

Figure 5 shows the prediction profiler for 19-pax aircraft with Architecture 1. The main hybridization benefit is evaluated in terms of block fuel savings and a baseline value (blue line) of 402 kg for the ATA is shown for comparison purposes. Based on the best design represented by the set of design variables shown in Fig. 5, the block fuel is reduced by 2.78%. This reduction is achieved from a moderate level of electrification of 15% (relative to the sample range), represented in the profiler by the sea-level electric power fraction design variable. At the aircraft level, the achieved fuel savings are accomplished with an increase in the TOGW and OEW by 3.02% and 1.49% respectively in comparison to the ATA, mainly due to the additional weight of the battery (157 kg). By inspecting the trends using the prediction profiler, given the 2030 technology assumptions in Table 9, the powertrain design variables that have the most significant impacts on vehicle sizing and performance are the sea-level electric power fraction, the climb boost strategy, the total climb boost altitude, and the E-taxi switch.

As a direct driving factor in the sizing of engines and electric motors, the sea-level electric power fraction has a strong impact on the time-to-climb, BSFC, battery weight, OEW, and TOGW. Since a partial climb boost is used, downsized engines due to higher electric power fraction will lead to a longer time to climb. As the engines become downsized, they tend to operate closer to the maximum power setting during the cruise, making them more fuel efficient, hence lower BSFC. However, as the electric motors are upsized, more battery energy is required, resulting in a rapid increase in battery weight, along with an increase in OEW and TOGW.

As for the climb boost, with downsized engines due to moderate electrification, a low-altitude boost with the electric motors operating at 95% power is required to satisfy the sea level rate of climb requirement (no less than 2140 ft/min). While increasing the total climb boost altitude helps reduce the time to climb, a higher battery energy requirement also causes an increase in block fuel and TOGW.

The E-taxi switch primarily has an impact on block fuel reduction (approximately 3%). This is achieved by avoiding

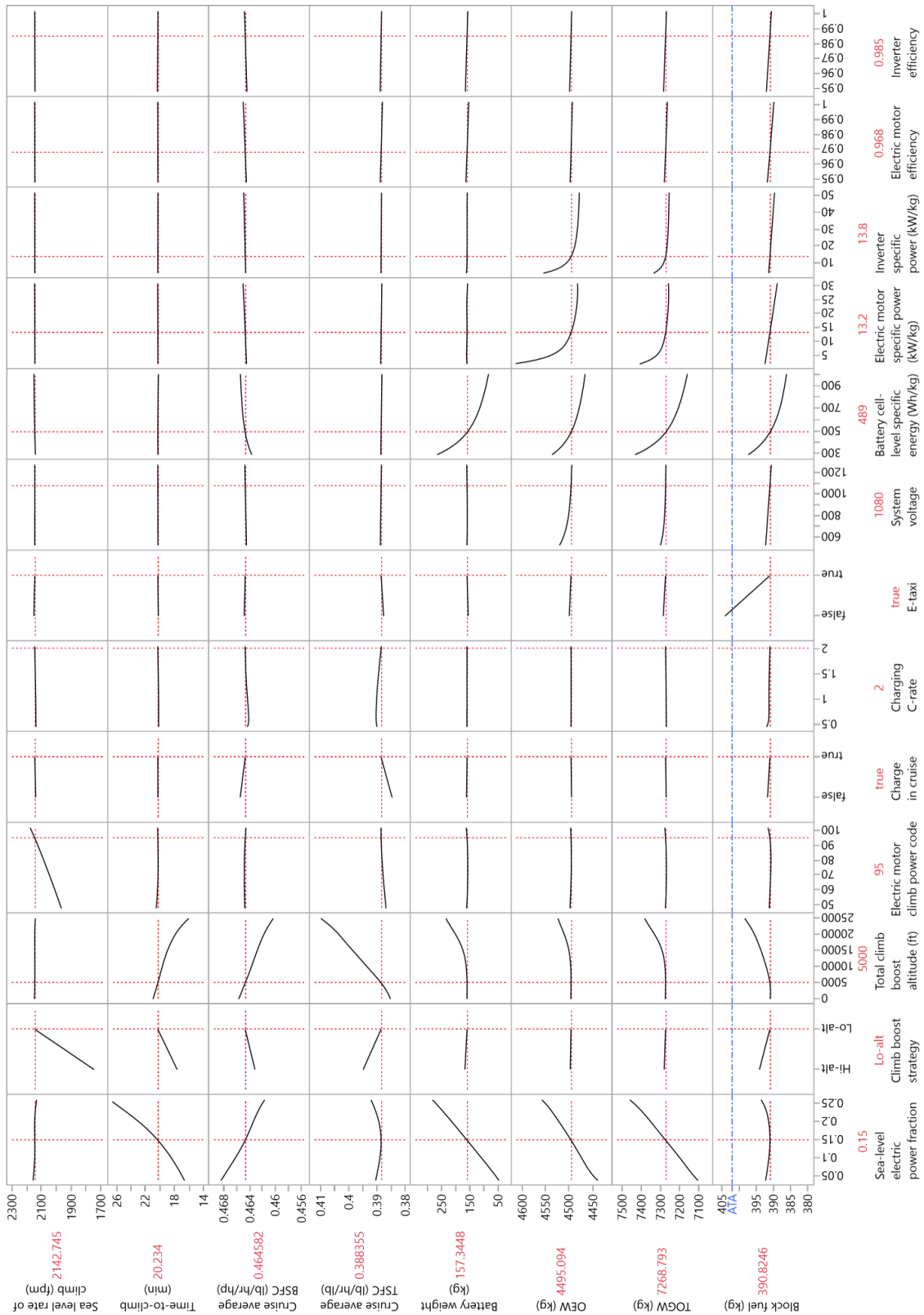


Fig. 5 Prediction profiler for 19-pax with Architecture 1

running the engines near idle power where the fuel efficiency is much worse than the cruise condition. The additional battery upsizing is negligible due to the relatively short duration and low power requirement.

The in-flight charging parameters do not have a significant impact on vehicle sizing and performance since the battery is relatively small and does not require much additional fuel burn to recharge. Their primary impacts are seen on the BSFC and TSFC: when recharging in cruise is desired, the BSFC improves (reduces) since the engines run at higher power settings to recharge the battery, but the TSFC becomes higher since more fuel is burned without generating more thrust. The system voltage has a minor impact on TOGW and block fuel: as the system voltage increases, cables and wires become lighter.

Among the electric component technology variables, the battery specific energy has the most significant impact on weights and block fuel. The specific power and efficiency of the electric motors and inverters have a less significant impact on vehicle sizing. Technology improvements will lead to diminishing returns, which is represented by a reduction in the absolute value of the slopes in the profiler cells.

2. 50-pax Vehicle with Architecture 1

Figure 6 shows the prediction profiler for the 50-pax vehicle with Architecture 1. The best design achieves 2.4% block fuel reduction compared to the ATA (744 kg) with a relatively low sea-level electric power fraction of 0.05. The impacts of the powertrain design variables except the sea-level electric power fraction are similar to the 19-pax results. In order to satisfy the sea-level rate of climb requirement, a low-altitude boost with electric motors operating at 89% power is required. A total climb boost altitude of 10 500 ft minimizes the OEW, the TOGW, and the design mission block fuel. Recharging in cruise improves the BSFC but worsens the TSFC since the engines operate at more efficient power settings but the propellers do not generate more thrust. By avoiding operating the engines at inefficient idle power settings, E-taxi contributes to a 2.0% fuel saving without significant impact on the TOGW and the OEW.

The impacts of sea-level electric power fraction (λ_{SL}) can be seen as piecewise functions based on Fig. 6. Due to the relatively low vehicle power-to-weight ratio (P_{TO}/W_0) of the 50-pax ATA, the gas turbine engines cannot be downsized significantly in order not to violate the top-of-climb and cruise power requirements. These constraints translate to a usable upper bound of $\lambda_{SL} \approx 0.1$. When $\lambda_{SL} < 0.1$, the engines and the electric motors are sized such that the total sea level power available matches exactly the takeoff power requirement, i.e., the equalities in Eq. (1) and (2). When $\lambda_{SL} > 0.1$, while the electric motors are still sized based on the equality in Eq. (2), the engines have to be oversized for takeoff to satisfy the top-of-climb and cruise power requirements, which results in a heavier powertrain. While the oversized engines improve the climb performance, the OEW, TOGW, and block fuel increase with steeper slopes when $\lambda_{SL} > 0.1$ as shown in Fig. 6, making such designs economically impractical.

3. 19-pax Vehicle with Architecture 2

Figure 7 shows the prediction profiler for 19-pax aircraft with Architecture 2. Unlike Architecture 1, Architecture 2 allows the use of electric motors during the cruise, therefore can support a significantly higher degree of electrification. Within the design space, the optimal sea-level electric power fraction to minimize block fuel is 30%, and the optimal cruise thrust split is 37%. Such a design achieves a 7.35% block fuel saving compared to the ATA. Similar to Architecture 1, E-taxi brings a fuel saving of about 5.6%. However, as indicated in Fig. 7, when E-taxi is desired, a minimum sea-level electric power fraction of 0.135 is required to satisfy the taxi thrust requirement.

Among the powertrain design variables, the sea-level electric fraction and the cruise target thrust split have the most significant impact on TOGW and block fuel. As in Architecture 1, the sea-level electric power fraction determines the sizing of turboprop engines and electric motors. Unique to Architecture 2, the cruise thrust split affects the power settings of engines and motors, thus the amount of fuel and battery energy consumed during cruise. A higher electric power fraction and cruise thrust split tend to consume more battery energy, therefore both the battery weight and the TOGW increase monotonically with these design variables. As the cruise thrust split increases, the engines tend to operate at low power settings, resulting in an increase in the BSFC; meanwhile, since a higher fraction of thrust required is generated by the motor-driven propellers, a significant decrease in the TSFC is observed.

Based on Fig. 7, a piecewise trend is observed in all responses with respect to the sea level electric power fraction and the cruise target thrust split. When the sea-level electric power fraction is held at 0.3, the two motor-driven propellers can provide up to approximately 65% of the cruise thrust required. Therefore, all outputs do not vary with the cruise target thrust split beyond 0.65. Similarly, when it is desired that the electric motors generate 37% of cruise thrust, a minimum sea-level electric power fraction of approximately 0.16 is required, below which the electric motors are undersized, and the actual cruise thrust split will deviate from the target value.

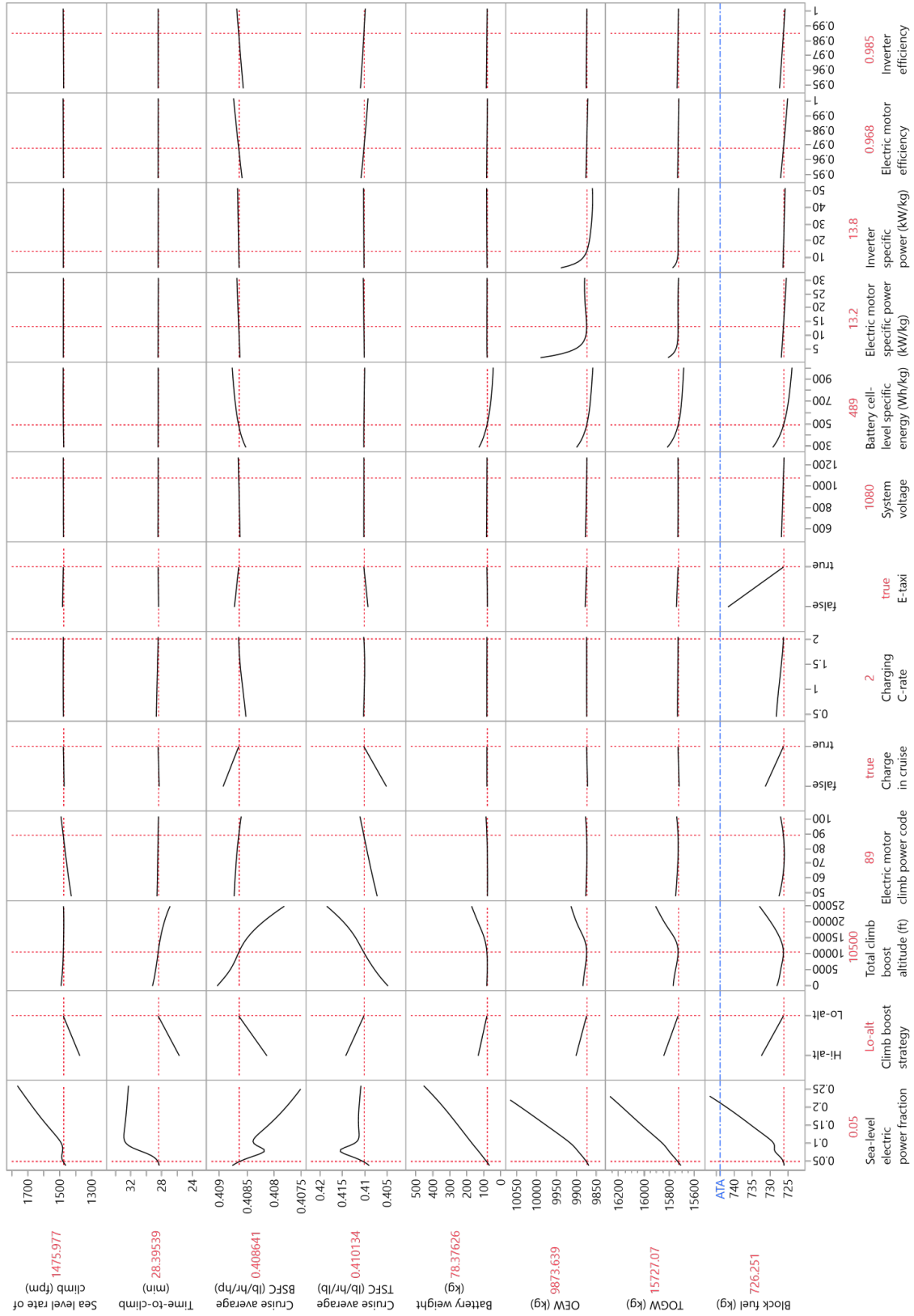


Fig. 6 Prediction profiler for 50-pax with Architecture 1

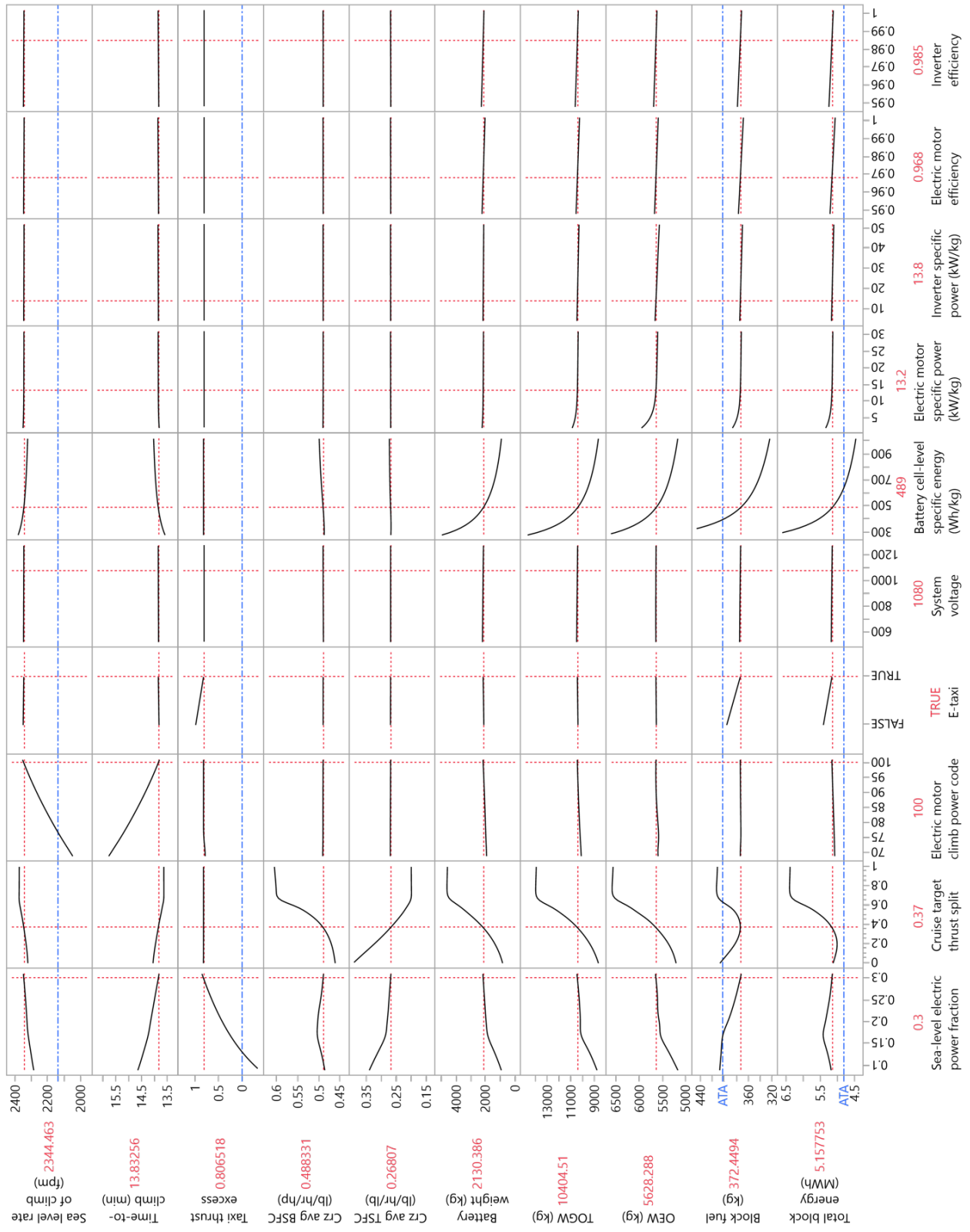


Fig. 7 Prediction profiler for 19-pax with Architecture 2

Due to a higher sea-level electric power fraction, the engines alone may not provide sufficient power during the climb, therefore Architecture 2 always boosts the entire climb segment. In order to satisfy the climb performance requirement, the electric motors should operate at a minimum of 75% of the rated power. However, since the climb motor power code has negligible impacts on weights and block fuel, it may be preferred to operate the electric motors at full power to further improve the climb performance.

Regarding the electrical components KPP variables, the battery cell specific energy has a more significant impact on fuel burn, energy consumption, and aircraft weight than the specific powers of the electric motor and inverter due to the extensive use of electric motors. This implies that the performance of Architecture 2 is very sensitive to the battery technology level. Similar to Architecture 1, a diminishing return is observed for all the technology variables.

4. 50-pax Vehicle with Architecture 2

Figure 8 presents the prediction profiler for the 50-pax model with Architecture 2. The optimal design achieves a fuel saving of 5.94%, featuring a high sea-level electric power fraction of 0.3 and a moderate cruise thrust split of 0.33. Overall, the impacts of powertrain design variables are similar to the 19-pax results.

Since the electric motors do not lapse with airspeed and altitude, as the sea-level electric power fraction increases, the sea-level rate of climb increases, and the total time-to-climb decreases. Given the 2030 battery specific energy assumption, the battery weight, TOGW, and OEW increase monotonically due to an increasing electric energy requirement. Meanwhile, block fuel monotonically decreases within the sample range. As the cruise target electric power fraction increases, the motor-driven propellers tend to provide a larger fraction of thrust, while the engines tend to operate at lower power settings. Therefore, the BSFC increases but the TSFC decreases. Due to the increased electric energy requirement, the battery weight, TOGW, and OEW increase more significantly compared to the impact of sea-level electric power fraction. Similar to the 19-pax results, both the sea-level electric power fraction and the cruise target thrust split have a piece wise impact on the outputs. When the sea-level electric power fraction is held at 0.3, the motor-driven propellers can supply no more than 55% of the cruise thrust required. When the motor-driven propellers are required to supply 33% of the cruise thrust, a minimum sea-level electric power fraction of 0.18 is necessary.

The electric motor power code during the climb mainly affects the climb performance. With the sea-level electric power fraction being 0.3, the electric motors need to operate at a minimum of 82% of rated power in order to satisfy the sea-level rate of climb requirement. However, since the electric motor power code during the climb does not have a significant impact on weights and block fuel, it may be preferred to operate the motors at full power to further improve the climb performance.

The use of E-taxi brings a notable fuel saving of 3.9% since the engines are turned off instead of being operated at inefficient near-idle conditions. Although E-taxi requires an upsized battery to provide additional electric energy, the impact on TOGW and OEW is negligible. Since the motor-driven propellers are smaller than the engine-driven propellers and the propellers in Architecture 1 (given the same TOGW), if E-taxi is desired, the 50-pax requires a minimum sea-level electric power fraction of 0.165 in order to satisfy the taxi thrust requirement.

Regarding the component KPP variables, the battery specific energy remains the most impactful factor for weights and block fuel, since the architecture is expected to consume more electric energy compared to the first architecture due to a higher degree of electrification and cruise hybridization. On the other hand, increasing the specific power of electric motors and inverters brings marginal improvements at most vehicle-level performance metrics except that the block fuel can be improved slightly by increasing the component efficiency.

C. Optimal EAP Designs

The settings in Figs. 5 through 8 establish the optimal designs of the aforementioned EAP architectures which minimize the design mission block fuel with the common 2030 technological assumptions in Table 9, subject to the constraint of the sea-level rate of climb and taxi thrust requirement. Tables 10 and 11 present the vehicle-level metrics of the optimal designs and the effects of electrification over the respective ATA models. These selected designs are re-evaluated in the M&S environment to eliminate prediction errors from the surrogate models.

Despite an increase in both the TOGW and OEW, all EAP optimal designs exhibit fuel savings over the respective ATA models. In general, Architecture 2 shows more fuel benefit compared to Architecture 1, since Architecture 1 only consumes battery energy for E-taxi, takeoff boost, and partial climb boost, but recharges the battery in flight, while Architecture 2 extends the battery usage to the entire climb, cruise, approach, and landing segments without in-flight recharging.

A comparison of the BSFC and TSFC reveals the different fuel-saving mechanisms between the two architectures.

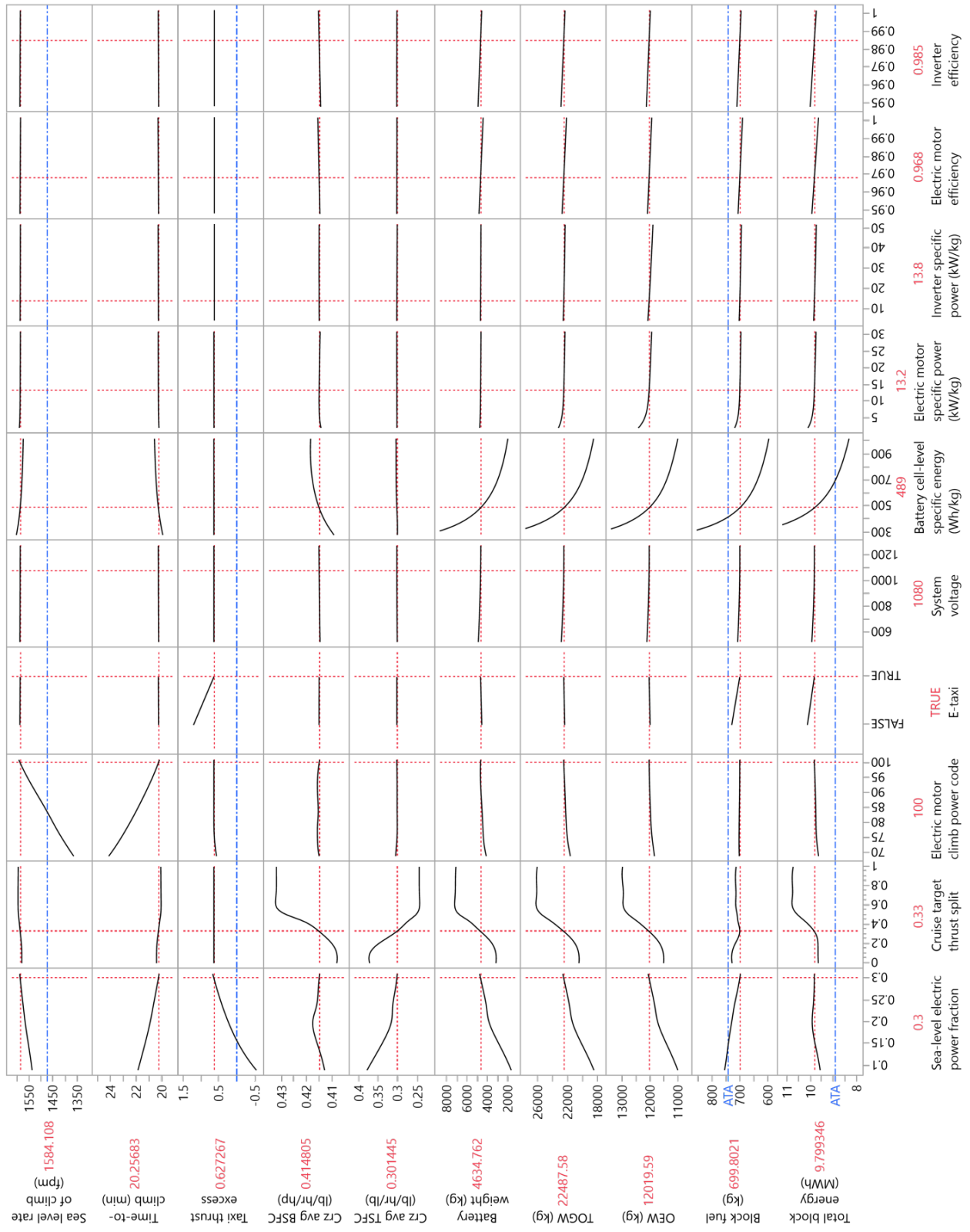


Fig. 8 Prediction profiler for 50-pax with Architecture 2

Table 10 Impacts of hybridization on the 19-pax aircraft with 2030 technology assumptions

Item	Unit	ATA	Architecture 1		Architecture 2	
		Value	Value	Change	Value	Change
Maximum takeoff weight	kg	7056	7269	+3.02%	10 405	+47.46%
Operating empty weight	kg	4429	4495	+1.49%	5628	+27.1%
Engine rated power	kW	823	720	-12.46%	849	+3.18%
Electric motor rated power	kW	N/A	127	N/A	146	N/A
Battery weight	kg	N/A	157	N/A	2130	N/A
Design mission block fuel	kg	402	391	-2.78%	373	-7.35%
Design mission block energy	MWh	4.820	4.688	-2.78%	5.158	+7.01%
Cruise average BSFC	lbm/hp/h	0.4713	0.4645	-1.44%	0.4883	+3.61%
Cruise average TSFC	lbm/lbf/h	0.3914	0.3883	+0.79%	0.2681	-31.5%

Table 11 Impacts of hybridization on the 50-pax aircraft with 2030 technology assumptions

Item	Unit	ATA	Architecture 1		Architecture 2	
		Value	Value	Change	Value	Change
Maximum takeoff weight	kg	15 654	15 727	+0.46%	22 488	+43.66%
Operating empty weight	kg	9846	9874	+0.28%	12 020	+22.08%
Engine rated power	kW	1252	1195	-4.55%	1259	+0.58%
Electric motor rated power	kW	N/A	63	N/A	540	N/A
Battery weight	kg	N/A	78	N/A	4635	N/A
Design mission block fuel	kg	744	726	-2.42%	700	-5.94%
Design mission block energy	MWh	8.921	8.705	-2.42%	9.799	+9.84%
Cruise average BSFC	lbm/hp/h	0.4090	0.4086	-0.10%	0.4148	+1.42%
Cruise average TSFC	lbm/lbf/h	0.4087	0.4101	+0.34%	0.3014	-26.25%

In Architecture 1, all cruise propulsive power is provided by the gas turbine engines. By boosting the takeoff and climb segments, the engines are downsized and can operate near the most efficient condition during the cruise. This improves the BSFC despite a slightly higher TSFC due to in-flight recharging, but the overall fuel benefit is small due to the top-of-climb and cruise power constraints on engine downsizing. Meanwhile, in Architecture 2, the electric motors complement the gas turbine engines during the cruise. This allows the engines to operate at low power settings, drastically reducing the TSFC at a cost of a relatively small increase in the BSFC. Although there is a significant increase in TOGW due to the large battery, the low TSFC of Architecture 2 still leads to a better fuel saving than Architecture 1.

From Tables 10 and 11, it is also observed that Architecture 2 on both vehicles requires a higher amount of block energy compared to the ATA since the additional electric energy consumed negates the energy saved in block fuel. Based on the prediction profilers in Figs. 7 and 8, in order to neutralize the impact on block energy, the battery cell-level specific energy should be at least 600 Wh/kg for the 19-pax vehicle and 680 Wh/kg for the 50-pax vehicle, which is around the predicted nominal 2040 technology levels [3]. While the block energy measures the total energy requirement to fly the mission, the block fuel is still used as the objective of minimization in this study, since the electric energy for recharging on the ground may be generated in cleaner ways that do not produce as much emission as burning jet fuel.

D. Impacts of Battery Technology on Optimal EAP Designs

The prediction profilers in Figs. 5 thru 8 indicate that the battery technology, characterized by the cell-level specific energy, has the strongest impact on weights, fuel burn, and total energy consumption among the electric component

KPP variables considered. Further investigation within the design space using the prediction profilers reveals that the optimal values of powertrain design variables also strongly depend on the battery specific energy.

1. Interaction between Battery Technology and Sea-Level Electric Power Fraction

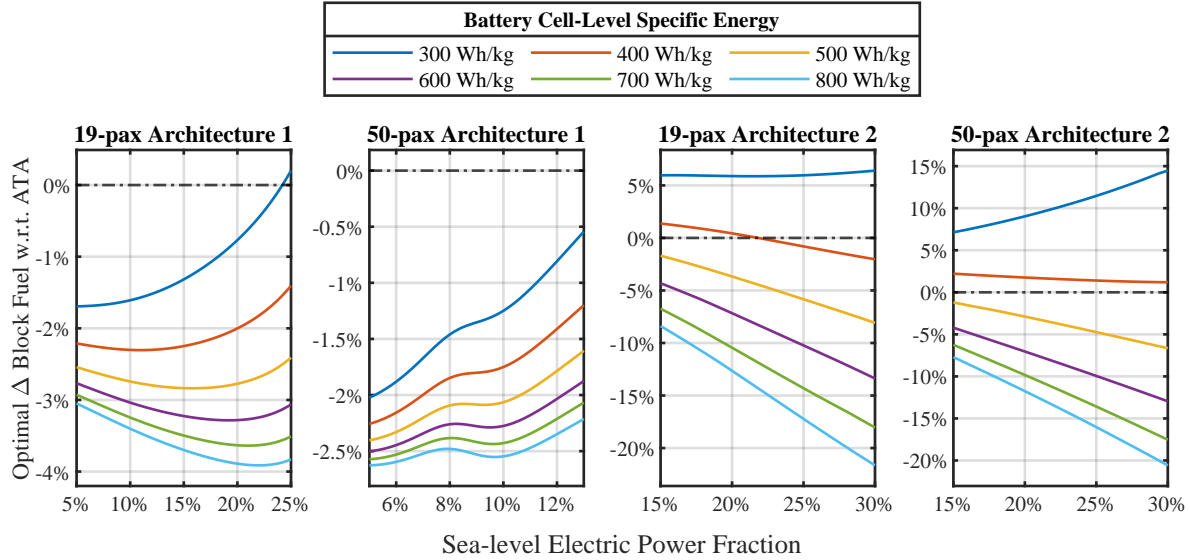


Fig. 9 Interaction between sea-level electric power fraction and battery specific energy (E-taxi = On)

Figure 9 presents the variation of block fuel with respect to the sea-level electric power fraction and battery cell-level specific energy. In all cases, E-taxi is preferred to minimize the block fuel. The interaction between the sea-level electric power fraction and battery specific energy can be observed from both the values and the slopes of the optimal block fuel response. For each model, as the battery specific energy increases, the optimal block fuel curve shifts downwards, indicating improved fuel performance due to a lighter battery pack. In the meantime, the slope at a given sea-level electric power fraction also decreases (becomes more negative), implying either less fuel penalty or more fuel benefit when the sea-level electric power fraction increases, since the battery mass grows more slowly with high specific energy. These effects, combined together, cause not only an improvement in fuel performance but also in general an increase in the optimal sea-level electric power fraction. An exception is the 50-pax vehicle with Architecture 1: as discussed earlier, due to its low vehicle power-to-weight ratio, the economically viable sea-level electric power fraction is limited below 10%, regardless of all other input variables; the optimal sea-level electric power fraction thus remains at a low level for a wide range of battery specific energy.

2. Sensitivity of Fuel Performance to Battery Technology and E-Taxi Strategy

Figure 10 presents the variation of the optimal block fuel with respect to the battery cell-level specific energy, which is created by connecting the points representing the minimum block fuel on each curve in Fig. 9 and recording their coordinates. For comparison, a curve with the E-taxi switch being “off” is also created in a similar way for each model.

Comparing the slopes of the curves between Architecture 1 and Architecture 2, it is observed that the fuel performance of Architecture 2 is much more sensitive to the battery technology than Architecture 1. For Architecture 2, since an extensive amount of electric energy is consumed during the cruise, the battery mass contributes to a significant part of the vehicle gross weight, especially at low specific energy. Therefore, while Architecture 1 may show more fuel benefit in the near term when the specific energy is low, Architecture 2 has a greater potential in the long term to achieve better fuel savings when battery technology improves.

It is also observed from Fig. 10 that the fuel saving due to E-taxi, represented by the vertical gap between the two curves, increases marginally with the battery specific energy. However, it is insensitive to the battery specific energy within the range considered. During the E-taxi, the propeller speed is varied to minimize the power requirement, and the efficiency of electric motors remains high for a wide range of power requirement and propeller speed. Therefore,

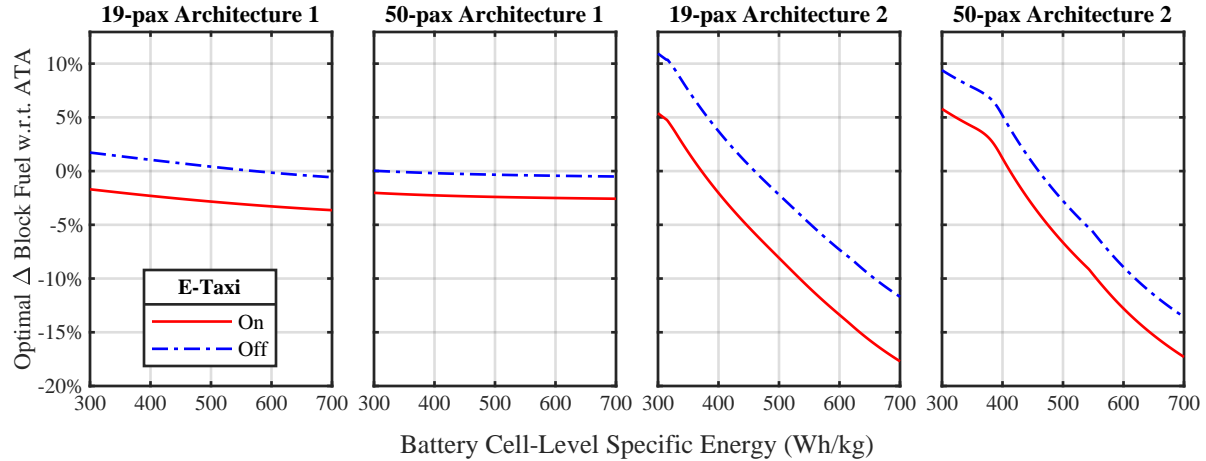


Fig. 10 Interaction between battery specific energy and E-taxi strategy

only a small amount of electric energy is required for E-taxi, which does not contribute to a large portion of the battery mass. Meanwhile, a more significant amount of fuel saving is resulted from avoiding running the engines at the most inefficient conditions in the entire mission, which is independent of the battery technology. Since the total duration of taxi segments is the same for both vehicles but the overall mission endurance is shorter for the 19-pax vehicle, the E-taxi shows more fuel benefit for the 19-pax vehicle compared to the 50-pax vehicle.

3. Impact of Battery Technology on Optimal Powertrain Design Variables

Figure 11 presents the variation of the optimal sea-level electric power fraction and (for Architecture 2 only) cruise target thrust split with respect to the battery cell-level specific energy. In each subfigure, the red solid curve indicates the sea-level electric power fraction or the cruise target thrust split which minimizes the block fuel. Two bands are plotted above and below the optimal curve indicating the maximum deviation from the optimal values that result in 0.1% and 0.5% fuel penalty relative to the optimal designs, respectively.

With Architecture 1, the optimal sea-level electric power fraction for the 19-pax vehicle increases steadily from 5% to 21% as the cell-level specific energy increases from 300 Wh/kg to 700 Wh/kg. A large deviation in the sea-level electric power fraction can be accepted without significantly compromising the fuel performance. For example, at 489 Wh/kg, the sea-level electric power fraction may be reduced from 15% to 9.3% with a 0.1% increase in the block fuel; then, based on the prediction profiler in Fig. 5, the TOGW and the OEW (excluding battery) will be reduced by 1.2% and 0.57%, respectively. For the 50-pax vehicle, the optimal sea-level electric power fraction remains at 5% within the range of specific energy considered, and a fuel penalty band is not visible below the optimal curve within the design space; therefore, a more comprehensive study on an expanded design space may be necessary to investigate the trade-off between fuel saving and aircraft weights.

With Architecture 2, when the battery specific energy is low, the unconstrained optimal sea-level electric power fraction remains at the lower bound of the design space and the cruise target thrust split remains below 10%. At approximately 315 Wh/kg for the 19-pax vehicle and 370 Wh/kg for the 50-pax vehicle, the optimal sea-level electric power fraction increases steeply until hitting the upper bound, and the cruise target thrust split also increases steadily, implying a preference to use the battery energy. At high specific energy (above 450 Wh/kg), the block fuel optimality is sensitive to the sea-level electric power fraction, as implied by the narrow bands, and there is little margin to trade block fuel for TOGW and OEW. For example, for the 50-pax vehicle, at 489 Wh/kg, reducing the sea-level electric power fraction from 30% to 29.7% causes a fuel penalty of 0.1%, but the TOGW and OEW may only be reduced by 0.16% and 0.08%, respectively. Meanwhile, the block fuel optimality is less sensitive to the cruise target thrust split as indicated by the wider bands in the third column of Fig. 11. For the 50-pax vehicle, at 489 Wh/kg, reducing the cruise thrust split from 33% to 31% causes a fuel penalty of 0.1%, and the TOGW and OEW can be reduced by 1.3% and 0.63%, respectively. Therefore, if the aircraft weights are of greater concern during the design process, it is preferred to reduce the cruise target thrust split to avoid excessive fuel penalty.

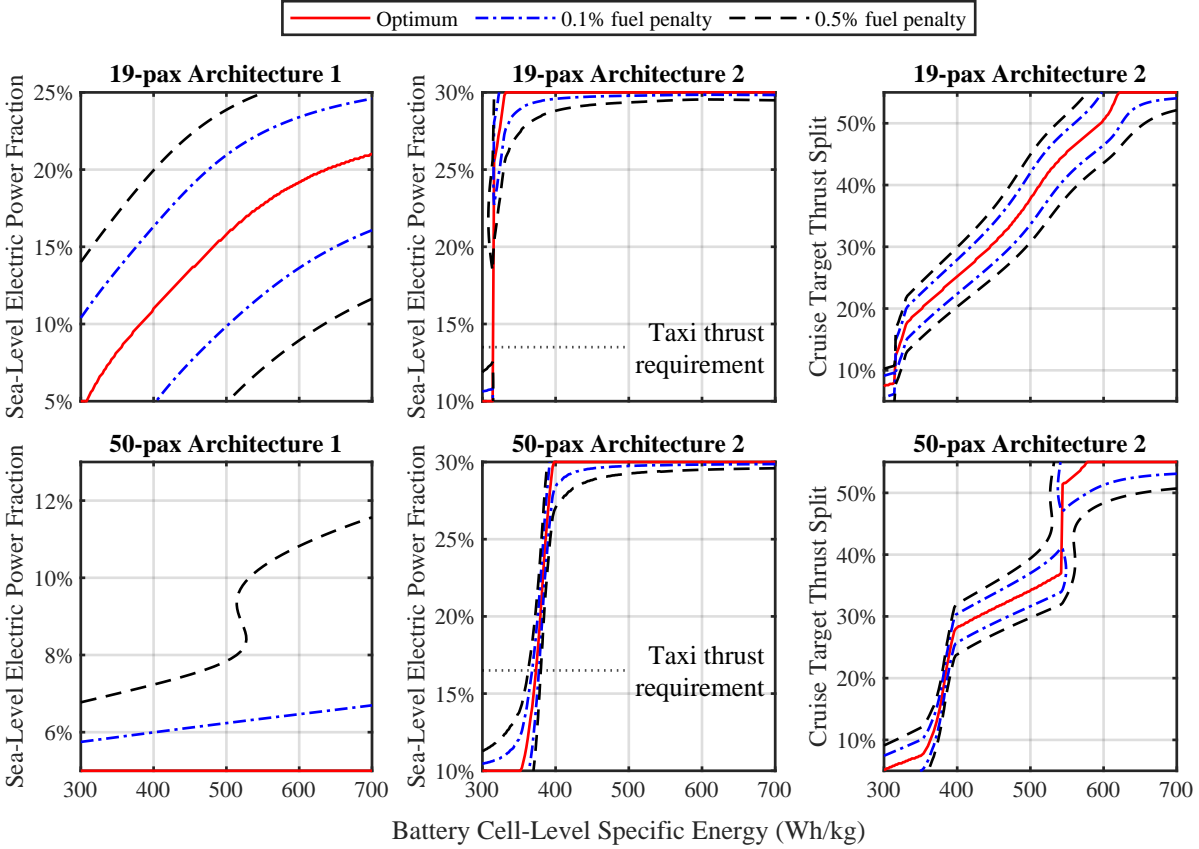


Fig. 11 Impact of battery specific energy on optimal sea-level electric power fraction and cruise target thrust split (E-taxi = On)

VI. Conclusion

This paper presents a design space exploration study to investigate the impact of applying hybrid parallel propulsion architectures on turboprop aircraft. Two baseline TRA models are established based on Beechcraft 1900D (19-pax size class) and ATR 42-600 (50-pax size class). To isolate the impact of hybridization on aircraft performance, ATA models are created by infusing 2030 airframe and engine technologies into the TRA models. Two parallel hybrid propulsion architectures are proposed: Architecture 1 maintains the baseline two-propeller configuration and installs an electric motor in parallel with each engine, and allows in-flight charging during cruise and descent; Architecture 2 is equipped with four propellers, each driven by an engine or an electric motor, and allows the use of electric motors during the cruise to complement the engines. Each architecture is parameterized with powertrain design variables, which describe the sizing and operating strategy of the hybrid powertrain, and electric component KPPs, which model the electric component technologies.

Enabled by the techniques of Design of Experiments and surrogate modeling, a design space exploration is performed on the powertrain design variables and the electric component KPPs. Each candidate is resized to maintain the same vehicle power-to-weight ratio, takeoff wing loading, and design mission as the respective ATA model. A constrained optimization on the design mission block fuel shows that given the 2030 electric technology assumptions, Architecture 1 achieves a small fuel saving (2.78% for 19-pax and 2.42% for 50-pax) by downsizing the engines and operating the engines at more efficient power settings during the cruise, while Architecture 2 achieves a better fuel saving (7.35% for 19-pax and 5.94% for 50-pax) with extensive use of electric energy during the cruise and operating the engines at low power settings. The use of E-taxi consistently results in a block fuel saving for both architectures and both vehicles when the battery technology is beyond the 2030 level. A preliminary sensitivity analysis reveals that, as the battery technology improves, the optimal degree of hybridization, as represented by the sea-level electric power fraction and (for Architecture 2 only) the cruise target thrust split, tends to increase in general, and the performance of Architecture 2

is more sensitive to the battery technology compared to Architecture 1 due to its extensive use of battery energy during the cruise.

Avenues of future work include the following: 1) Identify a set of Pareto optimal designs considering multiple objectives in addition to the block fuel, such as emission and energy cost [19]; 2) Evaluate the payload-range performance and assess the fuel and energy consumption of off-design missions [19]; 3) Study the impact of hybridization on secondary power subsystems, such as the sizing of the thermal management system [49] and the operability of hydraulic and pneumatic systems during E-taxi; 4) Incorporate certification requirements to constrain the power split optimization and propulsor positioning for the distributed propulsion of Architecture 2 [50]; 5) Apply the design and analysis process to hybrid architectures with other forms of energy storage, such as supercapacitors and fuel cells.

Acknowledgments

The authors would like to thank NASA for their support of this effort under AWD-002344 (NIA-602015), especially Gaudy Bezos-O'Connor, Ralph Jansen, and Fayette Collier.

References

- [1] Brelje, B. J., and Martins, J. R., "Electric, hybrid, and turboelectric fixed-wing aircraft: A review of concepts, models, and design approaches," *Progress in Aerospace Sciences*, Vol. 104, 2019, pp. 1–19. <https://doi.org/10.1016/j.paerosci.2018.06.004>.
- [2] Gao, Z., Kampezidou, S. I., Behere, A., Puranik, T. G., Rajaram, D., and Mavris, D. N., "Multi-level aircraft feature representation and selection for aviation environmental impact analysis," *Transportation Research Part C: Emerging Technologies*, Vol. 143, 2022, p. 103824. <https://doi.org/10.1016/j.trc.2022.103824>.
- [3] Tiede, B., O'Meara, C., and Jansen, R., "Battery Key Performance Projections based on Historical Trends and Chemistries," *2022 IEEE Transportation Electrification Conference & Expo (ITEC)*, IEEE, 2022. <https://doi.org/10.1109/itec53557.2022.9814008>.
- [4] Pastra, C. L., Hall, C., Cinar, G., Gladin, J., and Mavris, D. N., "Specific Power and Efficiency Projections of Electric Machines and Circuit Protection Exploration for Aircraft Applications," *2022 IEEE Transportation Electrification Conference & Expo (ITEC)*, IEEE, 2022. <https://doi.org/10.1109/itec53557.2022.9813927>.
- [5] Hall, C., Pastra, C. L., Burrell, A., Gladin, J., and Mavris, D. N., "Projecting Power Converter Specific Power Through 2050 for Aerospace Applications," *2022 IEEE Transportation Electrification Conference & Expo (ITEC)*, IEEE, 2022. <https://doi.org/10.1109/itec53557.2022.9813991>.
- [6] Mukhopadhyaya, J., and Graver, B., *Performance Analysis of Regional Electric Aircraft*, International Council on Clean Transportation, 2022. URL <https://theicct.org/wp-content/uploads/2022/07/global-aviation-performance-analysis-regional-electric-aircraft-jul22-1.pdf>.
- [7] Bravo, G. M., Praliyev, N., and Árpád Veress, "Performance analysis of hybrid electric and distributed propulsion system applied on a light aircraft," *Energy*, Vol. 214, 2021, p. 118823. <https://doi.org/https://doi.org/10.1016/j.energy.2020.118823>, URL <https://www.sciencedirect.com/science/article/pii/S0360544220319307>.
- [8] Felder, J. L., "NASA electric propulsion system studies," Tech. rep., NASA, 2015.
- [9] Sahoo, S., Zhao, X., and Kyprianidis, K., "A Review of Concepts, Benefits, and Challenges for Future Electrical Propulsion-Based Aircraft," *Aerospace*, Vol. 7, No. 4, 2020. <https://doi.org/10.3390/aerospace7040044>, URL <https://www.mdpi.com/2226-4310/7/4/44>.
- [10] Fornaro, E., Cardone, M., and Dannier, A., "A Comparative Assessment of Hybrid Parallel, Series, and Full-Electric Propulsion Systems for Aircraft Application," *IEEE Access*, Vol. 10, 2022, pp. 28808–28820. <https://doi.org/10.1109/ACCESS.2022.3158372>.
- [11] Pastra, C. L., Dull, C., Berumen, R., Yumuk, C., Cinar, G., and Mavris, D. N., "Viability Study of an Electrified Regional Turboprop," *2022 IEEE Transportation Electrification Conference Expo (ITEC)*, 2022, pp. 231–236. <https://doi.org/10.1109/ITEC53557.2022.9813756>.
- [12] (PIPISTREL), F. G., (POLIMI), L. T., (POLIMI), A. R., and (PIPISTREL), I. P., *Concept of Modular Architecture for Hybrid Electric Propulsion of Aircraft*, Modular Approach to Hybrid Electric Propulsion Architecture, 2017. URL <https://mahepa.eu/wp-content/uploads/2017/12/D1.1-Concept-of-Modular-Architecture-fro-Hybrid-Electric-Propulsion-of-Aircraft.pdf>.

- [13] Jimenez, D., Valencia, E., Herrera, A., Cando, E., and Pozo, M., "Evaluation of Series and Parallel Hybrid Propulsion Systems for UAVs Implementing Distributed Propulsion Architectures," *Aerospace*, Vol. 9, No. 63, 2022. <https://doi.org/https://doi.org/10.3390/aerospace9020063>.
- [14] Spierling, T., and Lents, C., "Parallel Hybrid Propulsion System for a Regional Turboprop: Conceptual Design and Benefits Analysis," *2019 AIAA/IEEE Electric Aircraft Technologies Symposium (EATS)*, 2019, pp. 1–7. <https://doi.org/10.2514/6.2019-4466>.
- [15] Lambe, A. B., and Martins, J. R. R. A., "Extensions to the design structure matrix for the description of multidisciplinary design, analysis, and optimization processes," *Structural and Multidisciplinary Optimization*, Vol. 46, No. 2, 2012, pp. 273–284. <https://doi.org/10.1007/s00158-012-0763-y>.
- [16] McCullers, L., *Flight Optimization System, Release 8.11, User's Guide*, NASA Langley Research Center, Hampton, VA 23681-0001, Oct. 2009.
- [17] Wells, D. P., Horvath, B. L., and McCullers, L. A., "The Flight Optimization System Weights Estimation Method," Tech. rep., NASA, Jun. 2017.
- [18] Cai, Y., Rajaram, D., and Mavris, D. N., "Multi-mission Multi-objective Optimization in Commercial Aircraft Conceptual Design," *AIAA Aviation 2019 Forum*, American Institute of Aeronautics and Astronautics, 2019. <https://doi.org/10.2514/6.2019-3577>.
- [19] Cai, Y., Rajaram, D., and Mavris, D. N., "Simultaneous aircraft sizing and multi-objective optimization considering off-design mission performance during early design," *Aerospace Science and Technology*, 2022, p. 107662. <https://doi.org/10.1016/j.ast.2022.107662>.
- [20] Lytle, J. K., "The Numerical Propulsion System Simulation: An Overview," Tech. Rep. NASA/TM-2000-209915, National Aeronautics and Space Administration, Glenn Research Center, Cleveland, OH, June 2000.
- [21] Cinar, G., "A Methodology For Dynamic Sizing of Electric Power Generation and Distribution Architectures," Ph.D. thesis, Georgia Institute of Technology, 2018.
- [22] Cinar, G., Garcia, E., and Mavris, D. N., "A framework for electrified propulsion architecture and operation analysis," *Aircraft Engineering and Aerospace Technology*, Vol. 92, No. 5, 2019, pp. 675–684. <https://doi.org/10.1108/aeat-06-2019-0118>.
- [23] *Model 1900D Airliner Pilot's Operating Manual*, Hawker Beechcraft Corporation, P.O. Box 85, Wichita, Kansas, 67201-0085 USA, Sep. 2008.
- [24] "TYPE-CERTIFICATE DATA SHEET for PT6A-67 Series Engines," online, Oct. 2019. URL https://www.easa.europa.eu/sites/default/files/dfu/PT6A_67%20Series%20Issue%2005_20191011.pdf.
- [25] ATR, "ATR 42-600," Online, 2020. URL https://www.atr-aircraft.com/wp-content/uploads/2020/07/Factsheets_-_ATR_42-600.pdf.
- [26] "TYPE-CERTIFICATE DATA SHEET for PW100 series engines," online, Mar. 2018. URL <https://www.easa.europa.eu/sites/default/files/dfu/EASA%20IM.E.041%20TCDS%20Issue%204.pdf>.
- [27] Cai, Y., Xie, J., Cinar, G., and Mavris, D. N., "Advanced 2030 Turboprop Aircraft Modeling for the Electrified Powertrain Flight Demonstration Program," *2022 IEEE Transportation Electrification Conference & Expo (ITEC)*, IEEE, 2022. <https://doi.org/10.1109/itec53557.2022.9813858>.
- [28] Mavris, D. N., Tai, J., and Gladin, J., "FY2019 Advanced Air Transportation Technologies Systems Analysis Report: Technology Portfolio," techreport, Georgia Institute of Technology, Jul. 2020.
- [29] Catalano, P., de Rosa, D., Mele, B., Tognaccini, R., and Moens, F., "Performance Improvements of a Regional Aircraft by Riblets and Natural Laminar Flow," *Journal of Aircraft*, Vol. 57, No. 1, 2020, pp. 29–40. <https://doi.org/10.2514/1.c035445>.
- [30] Horstmann, K.-H., Mueller, R., Rohardt, C.-H., Quast, A., Echtle, H., Wohlrath, W., Dick, P., Welte, D., and Stock, H., "Design and Flight Test Evaluation of a Laminar Wing Glove on a Commuter Aircraft," ICAS, 1994.
- [31] Urnes, J., and Nguyen, N., "A Mission Adaptive Variable Camber Flap Control System to Optimize High Lift and Cruise Lift to Drag Ratios of Future N+3 Transport Aircraft," *51st AIAA Aerospace Sciences Meeting including the New Horizons Forum and Aerospace Exposition*, American Institute of Aeronautics and Astronautics, 2013. <https://doi.org/10.2514/6.2013-214>.

- [32] Ippolito, C. A., Nguyen, N. T., Totah, J., Trinh, K., and Ting, E. B., "Initial Assessment of a Variable-Camber Continuous Trailing-Edge Flap System for Drag-Reduction of Non-Flexible Aircraft in Steady-State Cruise Condition," *AIAA Infotech@Aerospace (I@A) Conference*, American Institute of Aeronautics and Astronautics, 2013. <https://doi.org/10.2514/6.2013-5143>.
- [33] Kundu, A., Watterson, J., and Raghunathan, S., "A multi-disciplinary study of aircraft aerodynamic surface smoothness requirements to reduce operating cost," *7th AIAA/USAF/NASA/ISSMO Symposium on Multidisciplinary Analysis and Optimization*, American Institute of Aeronautics and Astronautics, 1998. <https://doi.org/10.2514/6.1998-4874>.
- [34] Elkoby, R., Brusniak, L., Stoker, R., Khorrami, M., Abeyinghe, A., and Moe, J., "Airframe Noise Test Results from the QTD II Flight Test Program," *13th AIAA/CEAS Aeroacoustics Conference (28th AIAA Aeroacoustics Conference)*, American Institute of Aeronautics and Astronautics, 2007. <https://doi.org/10.2514/6.2007-3457>.
- [35] Takeda, N., Minakuchi, S., and Okabe, Y., "Smart composite sandwich structures for future aerospace application-Damage detection and suppression-: A review," *Journal of Solid Mechanics and Materials Engineering*, Vol. 1, No. 1, 2007, pp. 3–17.
- [36] Hou, T.-H., Baughman, J. M., Zimmerman, T. J., Sutter, J. K., and Gardner, J. M., "Evaluation of sandwich structure bonding in out-of-autoclave processing," *SAMPE Technical Conference*, 2010.
- [37] Snyder, C. A., and Tong, M. T., "Modeling Turboshift Engines for the Revolutionary Vertical Lift Technology Project," *75th Annual Vertical Flight Society (VFS 2019) Forum and Technology Display, Philadelphia*, 2019.
- [38] Antcliff, K. R., Guynn, M. D., Marien, T., Wells, D. P., Schneider, S. J., and Tong, M. J., "Mission Analysis and Aircraft Sizing of a Hybrid-Electric Regional Aircraft," *54th AIAA Aerospace Sciences Meeting*, American Institute of Aeronautics and Astronautics, 2016. <https://doi.org/10.2514/6.2016-1028>.
- [39] Cinar, G., Cai, Y., Denney, R. K., and Mavris, D. N., "Modeling and Simulation of a Parallel Hybrid Electric Regional Aircraft for the Electrified Powertrain Flight Demonstration (EPFD) Program," *2022 IEEE Transportation Electrification Conference & Expo (ITEC)*, IEEE, 2022. <https://doi.org/10.1109/itec53557.2022.9813832>.
- [40] *NFPA 70, National Electrical Code (NEC)*, National Fire Protection Association, 2017.
- [41] Cinar, G., Cai, Y., Bendarkar, M. V., Denney, R. K., and Mavris, D. N., "System Analysis and Design Space Exploration of Regional Aircraft with Electrified Powertrains," *AIAA SCITECH 2022 Forum*, American Institute of Aeronautics and Astronautics, 2022. <https://doi.org/10.2514/6.2022-1994>.
- [42] Cinar, G., Cai, Y., Bendarkar, M. V., Burrell, A. I., Denney, R. K., and Mavris, D. N., "System Analysis and Design Space Exploration of Regional Aircraft with Electrified Powertrains," *Journal of Aircraft*, 2022, pp. 1–28. <https://doi.org/10.2514/1.c036919>.
- [43] BETTNER, J., "Component arrangement studies for an 8000 shp turboshaft high technology core," *26th Joint Propulsion Conference*, 1990, p. 2398.
- [44] Vogt, R. L., and Sehra, A., "Next Generation 2 MW Turboshaft and Turbo Prop Engines," *Turbo Expo: Power for Land, Sea, and Air*, Vol. 78880, American Society of Mechanical Engineers, 1993, p. V001T01A005.
- [45] Gauntner, J. W., "ALGORITHM FOR CALCULATING TURBINE COOLING FLOW AND THE RESULTING DECREASE INTURBINE EFFICIENCY," Tech. Rep. NASA/TM-81453, National Aeronautics and Space Administration, 1980.
- [46] Schutte, J. S., "Simultaneous multi-design point approach to gas turbine on-design cycle analysis for aircraft engines," Ph.D. thesis, Georgia Institute of Technology, 2009.
- [47] Teeuwen, Y., "Propeller design for conceptual turboprop aircraft," mathesis, Delft University of Technology, Postbus 5, 2600 AA Delft, The Netherlands, Oct. 2017. URL <http://resolver.tudelft.nl/uuid:d746a647-25e1-463b-af3a-6c2c478e1b37>.
- [48] Hamilton Standard, "Generalized Method of Propeller Performance Estimation 1961-1963," , 1963. URL <https://open.bu.edu/handle/2144/10454>.
- [49] Shi, M., Sanders, M., Alahmad, A., Perullo, C., Cinar, G., and Mavris, D. N., "Design and Analysis of the Thermal Management System of a Hybrid Turboelectric Regional Jet for the NASA ULI Program," *AIAA Propulsion and Energy 2020 Forum*, American Institute of Aeronautics and Astronautics, 2020. <https://doi.org/10.2514/6.2020-3572>.
- [50] Xie, J., Cai, Y., Sarojini, D., Harrison, E., and Mavris, D. N., "Vertical Tail Sizing and Power Split Optimization for the PEGASUS Concept Considering Certification Requirements," *AIAA AVIATION 2022 Forum*, American Institute of Aeronautics and Astronautics, 2022. <https://doi.org/10.2514/6.2022-3204>.